Calculations for ^{4}He$(e,e'N)$

Dean Halderson
Department of Physics, Western Michigan University, Kalamazoo, Michigan 49008
(Received 13 October 1995)

Calculations have been performed for inelastic electron scattering from ^{4}He within the framework of the recoil-corrected continuum shell model. Comparisons are made to data ranging from q near zero to $q=650$ MeV/c. Both inclusive and exclusive processes have been investigated. The effect of meson exchange currents, spin-channel coupling, p-n channel coupling, relativistic corrections, and final state interactions are investigated. Agreement with data is generally good; however, the calculated inclusive transverse response is too small in the region of low energy transfer. This reduced strength is related to the lack of current conservation in the model. [S0556-2813(96)02906-8]

PACS number(s): 25.30.Fj, 21.60.Cs, 25.10.+s, 25.30.Dh

I. INTRODUCTION

The virtues of electroexcitation of nuclear states have been extolled for many years [1]. The knowledge that the electron interacts electromagnetically provides confidence in a single-scattering assumption. The ability to hold a constant energy transfer while varying the momentum transfer traces out the matrix elements of the nuclear current $J_\mu(\mathbf{q})$. Angular distributions provide a means of separating transverse and longitudinal contributions. The momentum dependence of the multipole operators allows identification of nuclear state spins and parities, and the excitation of high spin, unnatural parity states isolates the magnetization current.

Nucleon knockout further extends the knowledge available from inelastically scattered electrons. Under the assumptions that the struck nucleon moves in a mean field and that it does not interact with other particles after encountering the virtual photon, the coincidence cross section provides the momentum distribution for target nucleons.

Additional interest in scattering to the nuclear continuum has been generated by concerns about the suppression of the longitudinal response and predictions of nuclear transparency, and thus numerous theoretical and experimental investigations of both inclusive and exclusive reactions have been generated. Theoretical investigations have employed several techniques to describe the excitation process. Random phase approximation (RPA) calculations [2,3], resonating group (RGM) [4], continuum shell model [5,6], and optical model calculations, with both relativistic and nonrelativistic final states [7], have been used to describe inclusive and exclusive processes. In this paper the inclusive and exclusive processes will be investigated for ^{4}He with the recoil-corrected continuum shell model (RCCSM) [8].

This investigation was undertaken for several reasons. The first is to test the validity of approximations often employed in knockout reactions. The second is to see whether the model employed predicts suppression of the longitudinal form factor as have other calculations for ^{4}He. The third is to test whether coincidence measurements have the sensitivity to distinguish among ground state models of ^{4}He. The fourth is to determine the fraction of quasifree scattering due to single-nucleon knockout and that due to other processes. The fifth reason is that electroexcitation is part of a long term project to correlate data from various probes producing nucleon knockout from ^{4}He by comparison with RCCSM predictions. The RCCSM is ideal for such comparisons because the ingredients of the model are clear and can be cast in shell model terms.

The form of the model employed in this work can be visualized as a $1p$-$1h$ shell model in a translationally invariant basis. The proton and neutron particle state radial wave functions take the shape that solves the Hamiltonian for a given set of boundary conditions, and this translationally invariant Hamiltonian contains a realistic effective interaction with central, spin-orbit, and tensor components. The ^{4}He ground state is then a variational ground state, but one in which the trial wave function is fixed for the first two Jacobi coordinates and the third is restricted to $l=0$. It is, therefore, very naive compared to the sophisticated variational and Green function Monte Carlo calculations employing phenomenological two-nucleon potentials.

However, the model has desirable traits such as employing the same Hamiltonian for the ^{4}He ground state and the continuum states, thereby guaranteeing orthogonality, automatically including charge exchange, antisymmetrization, channel coupling, and final state interactions. These various mechanisms may be turned on and off to test their effects. It was shown in Ref. [8] that these mechanisms are essential in producing the excellent agreement with all ^{3}H$(p,p)^3$H, ^{3}He$(n,n)^3$He, and ^{3}H$(p,n)^3$He cross section, polarization, and analyzing power data below $E_N=70$ MeV [9]. The excellent agreement with these data provides confidence in the value of investigating other reactions. In addition, one is starting with continuum solutions that have a firmer theoretical basis than optical model wave functions, whose phase shifts may be equivalent, but which have different interior behavior and, in fact, must be orthogonalized to the ground state. With confidence in the continuum solutions, one can look for data that do not agree with RCCSM predictions and attempt to determine the structural complexities or omitted reaction mechanisms which cause the disagreement and, in some cases, identify data which are likely to be incorrect.

Because of the desire to correlate many data sets with one model, comparison is made to both inclusive and exclusive measurements at a variety of energies and momenta transferred. One would expect that the RCCSM cross sections

 © 1996 The American Physical Society

would be about 5% to 10% too high since the single-scattering assumption leads to cross sections proportional to the single-particle strength, and with no D state in the ^{4}He ground state wave function, the theoretical single-particle strength should be greater than the experimental strength. However, deviations from this expectation are found, most significantly at low energy and momentum transfer. Here, a comparison with inclusive data indicates that the longitudinal response is overpredicted in the calculation, while the transverse response is underpredicted. Whereas the large theoretical longitudinal response is likely due to a size effect, the small transverse response is unexplained. The imbalance between the space- and timelike current components means that the current is not conserved in the model. It is speculated that the lack of current conservation is due to missing shell model configurations, and this speculation will be pursued in future calculations.

At moderate momentum and energy transfer the calculated cross sections tend to be 10% to 15% lower than the experimental inclusive cross sections, but 20% higher than the experimental exclusive cross sections. Both the longitudinal and transverse exclusive responses are overpredicted by approximately the same amounts, showing that the present model predicts no suppression of the longitudinal response. A comparison of inclusive and exclusive data indicates that approximately one-third of the response between $q=300$ and 400 MeV/c is due to processes other than single-nucleon knockout.

Calculations were also performed for inclusive and exclusive cross sections with various mechanisms removed. Calculations omitting the continuum nucleon's interaction with the residual nucleus produced as much as a factor of 2 increase in cross sections at $q=300$ MeV/c. This demonstrates the type of error possible in plane-wave calculations. Channel coupling was also eliminated, producing 30% changes in the longitudinal response at low energy transfer. These results indicate some of the shortcomings of distorted-wave calculations.

Meson exchange currents contribute a fairly consistent 20% to the cross sections except at high missing momentum where the contribution may approach 40%. The second-order correction to the nonrelativistic transverse current operator can contribute as much as 20% at high energy transfer.

Finally, these calculations show that, at present, the information that can be gathered from comparisons between knockout experiments and sophisticated models of nuclear ground states appears to be limited. The two reasons for this conclusion are, first, that uncertainties are introduced by the use of distorted waves, especially at low energy transfer as described above, and, second, the RCCSM results, with its naive ground state, do as well in describing the data as those employing variational ground states.

II. FORMALISM

The RCCSM provides solutions to the ^{3}He$+n$, ^{3}H$+p$ coupled channels problem. The model is translationally invariant, fully antisymmetric, and employs a realistic effective interaction [10]. The structure of the residual nuclei is taken as $0s^3$, with the oscillator constant $\nu=0.36$ fm^{-2} fitted to the ^{3}H radius. The ^{4}He wave functions are then constructed by coupling the fourth particle to the three-particle core via coordinate ξ_3, as shown in Fig. 1. The harmonic oscillator basis functions are in the form

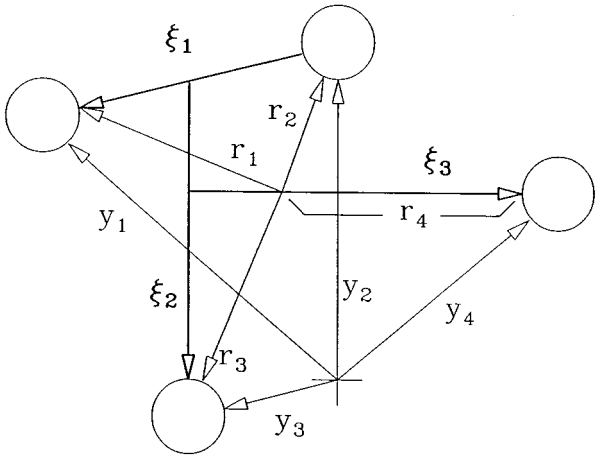

FIG. 1. The RCCSM coordinates.

$$\phi^{J_B M_B}_{\alpha n l j}(\xi) = (1-P_{34})/\sqrt{2}\,|0s^{\nu/2}(\xi_1)0s^{2\nu/3}(\xi_2)\chi^{1/2}_{\alpha}\Phi^{3\nu/4}_{nlj}(\xi_3)\tau_3\rangle^{J_B}_{M_B}, \tag{1}$$

where $\chi^{1/2}_{\alpha}$ is the ^{3}H or ^{3}He spin wave function.

The complete time reverse of a wave function with incoming flux v_i with initial conditions $i=\{\alpha J_A M_A m_s\}$ then takes the form [11]

$$\psi^{(-)}_i=(4\pi/p_i)\sum\,(i)^l Y^*_{lm_l}(\hat{\mathbf{p}})e^{-i\sigma_l} \times(-i/2)C^{l\,1/2\,j}_{m_l m_s m}C^{J_A j J_B}_{M_A m M_B}\Psi^{J_B M_B(-)}_c, \tag{2}$$

where the sum is over $lm_l jmJ_BM_B$ and

$$\psi^{J_B M_B(-)}_c=\sum_{c'}\,r^{-1}u^{J_B(-)}_{c'}(r)|\alpha' J'_A l' j' J_B M_B\rangle. \tag{3}$$

The radial function $u^{J_B(-)}_{c'}(r)$ has the asymptotic form

$$u^{J_B(-)}_{c'}(r)=u^{J_B(+)*}_{c'}\rightarrow(v_c/v_{c'})^{1/2}(O_{c'}\delta_{c'c}-I_{c'}S_{cc'}). \tag{4}$$

The index c stands for $\alpha J_A l j$ with J_A and j coupled to J_B, where J_A is the angular momentum of a possible core state, l and j are the nucleon orbital angular momentum and total angular momentum, respectively, p_i is the nucleon momentum in the nucleon-nucleus center of mass frame, and α represents other quantum numbers necessary to distinguish core states.

The notation for the nucleon knockout reaction in the laboratory system is as follows. The incident and exit electron momenta are $k_\mu=(k_0,\mathbf{k})$ and $k'_\mu=(k'_0,\mathbf{k}')$; the initial and final total nuclear momenta are $p_{B\mu}=(E_B,\mathbf{p}_B)$ and $p'_{B\mu}=(E'_B,\mathbf{p}'_B)$; the final, free nucleon momentum is $p_\mu=(p_0,\mathbf{p})$; the final core momentum is $p_{A\mu}=(E_A,\mathbf{p}_A)$; and the momen-

tum transferred to the nucleus is $q_\mu=(q_0,\mathbf{q})=k'_\mu-k_\mu$. The square of a four-vector is $q_\mu^2=q_0^2-q^2$, and $\omega=-q_0$.

Inclusive scattering requires integration over all possible outgoing channels and results in a cross section formula [6]

$$\frac{d^2\sigma}{d\Omega\ dE_x}=\frac{1}{2\pi}\sum_{c,J_B}(\mu_c/p_c)\frac{d\sigma_{cJ_B}}{d\Omega}, \tag{5}$$

where $d\sigma_{cJ_B}/d\Omega$ is a fictitious cross section calculated with wave functions in Eq. (3) with outgoing flux v_c in the open channel c. The equation for $d\sigma_{cJ_B}/d\Omega$ in the laboratory frame is the same as Eq. (3.65) in Ref. [1] for $m_e\approx 0$.

For exclusive scattering in the laboratory frame to a definite residual nuclear state, one has

$$\frac{d^5\sigma}{d\Omega\ d\Omega_p d\omega}=\frac{\alpha^2}{q_\mu^4}\left(\frac{2k'_0p_0p}{k_0R}\right)(k_\mu k'_\nu+k'_\mu k_\nu+q_\mu^2 g_{\mu\nu}/2)J^\mu J^{\nu *}. \tag{6}$$

In Eq. (6) α is the fine structure constant and R is part of the density of states,

$$R=(1-p_0\mathbf{p}\cdot\mathbf{p}_A/p^2E_A). \tag{7}$$

The nuclear currents in Eq. (6), $J_\mu=(\rho,\mathbf{J})$, are to be calculated with the wave functions in Eq. (2) divided by $(2\pi)^{3/2}$.

Conversion is then made to spherical tensors, $J_{\pm1}=\mp(J_x\pm iJ_y)$. The z axis is taken to a point along $\mathbf{q}$, which is the axis at quantization for $\mathbf{J}$, and the z' axis along $\mathbf{k}$, which is the axis of quantization for the nuclear states. At this point one may use the continuity equation $q_\mu J^\mu=0$ to eliminate J_z in favor of $(q_0/q)\rho$ as was done to obtain Eq. (3.65) in Ref. [1]. This point will be discussed below.

The spherical components of the nuclear currents are given by [1,12]

$$J_\lambda=-(2\pi)^{1/2}\sum_{JM}(-i)^J(2J+1)^{1/2}\langle J'_B\|-T_J^{\rm el}+\lambda T_J^{\rm mag}\|J_B\rangle \times(-)^{J'_B-M'_B}\begin{pmatrix}J'_B & J & J_B\\ -M'_B & M & M_B\end{pmatrix}D^J_{M\lambda}(0,\theta_q,0) \tag{8}$$

for $\lambda=\pm1$,

$$J_{\lambda=0}=J_z=(4\pi)^{1/2}\sum_{JM}(-i)^J(2J+1)^{1/2}\langle J'_B\|L_J\|J_B\rangle \times(-)^{J'_B-M'_B}\begin{pmatrix}J'_B & J & J_B\\ -M'_B & M & M_B\end{pmatrix}D^J_{M0}(0,\theta_q,0), \tag{9}$$

$$J_0=\rho=(4\pi)^{1/2}\sum_{JM}(-i)^J(2J+1)^{1/2}\langle J'_B\|M_J^{\rm Coul}\|J_B\rangle \times(-)^{J'_B-M'_B}\begin{pmatrix}J'_B & J & J_B\\ -M'_B & M & M_B\end{pmatrix}D^J_{M0}(0,\theta_q,0). \tag{10}$$

The D functions are those of Brink and Satchler [13] and rotate the system. ϕ_q is zero and ϕ_q is positive.

A nonrelativistic reduction on the current operators is employed [14,15]:

$$M_{JM}^{\rm Coul}=\sum_i\left\{j_J(qr_i)Y_{JM}(\hat{\mathbf{r}}_i)[F_1^i-q_\mu^2(F_1^i+2\kappa_iF_2^i)/8M_N^2]-(F_1^i+2\kappa_iF_2^i)/(\sqrt{2}q/4M_N)\left[\left(\frac{J+1}{2J+1}\right)^{1/2}\times j_{J+1}(qr_i)[Y_{J+1}(\hat{\mathbf{r}}_i)\otimes(\nabla_\xi\otimes\sigma)^1]_{JM}+\left(\frac{J}{2J+1}\right)^{1/2}j_{J-1}(qr_i)[Y_{j-1}(\hat{\mathbf{r}}_i)\otimes(\nabla_\xi\otimes\sigma)^1]_{JM}\right]\right\}, \tag{11}$$

$$T_{JM}^{\rm el}=\sum_i(F_1^i/M_N)\left\{-\left(\frac{J}{2J+1}\right)^{1/2}j_{J+1}(qr_i)[Y_{J+1}(\hat{\mathbf{r}}_i)\otimes\nabla_\xi]_{JM}+\left(\frac{J+1}{2J+1}\right)^{1/2}j_{J-1}(qr_i)[Y_{J-1}(\hat{\mathbf{r}}_i)\otimes\xi]_{JM}\right\} +[(F_1^i+\kappa_iF_2^i)/2M_N]qj_J(qr_i)[Y_J(\hat{\mathbf{r}}_i)\otimes\sigma_i]_{JM}+\sqrt{2}(F_1^i+2\kappa_iF_2^i)\omega/4M_N^2 \times\left\{-\left(\frac{J}{2J+1}\right)^{1/2}j_{J+1}(qr_i)[Y_{J+1}(\hat{\mathbf{r}}_i)\otimes(\nabla_\xi\otimes\sigma)^1]_{JM}+\left(\frac{J+1}{2J+1}\right)^{1/2}j_{J-1}(qr_i)[Y_{J-1}(\hat{\mathbf{r}}_i)\otimes(\nabla_\xi\otimes\sigma)^1]_{JM}\right\}, \tag{12}$$

$$T_{JM}^{\rm mag}=\sum_i(i/M_N)q\left\{-\left(\frac{J}{2J+1}\right)^{1/2}j_{J+1}(qr_i)[Y_{J+1}(\hat{\mathbf{r}}_i)\otimes\sigma_i]_{JM}+\left(\frac{J+1}{2J+1}\right)^{1/2}j_{J-1}(qr_i)[Y_{J-1}(\hat{\mathbf{r}}_i)\otimes\sigma_i]_{JM}\right\}[(F_1^i+\kappa_iF_2^i)/2M_N] -(iF_1^i/M_N)j_J(qr_i)[Y_J(\hat{\mathbf{r}}_i)\otimes\nabla_\xi]_{JM}-i\sqrt{2}[(F_1^i+2\kappa_iF_2^i)\omega/4M_N^2]j_J(qr_i)[Y_J(\hat{\mathbf{r}}_i)\otimes(\nabla_\xi\otimes\sigma)^1]_{JM}, \tag{13}$$

$$L_{JM}=\sum_i(F_1^i/M_N)\left\{\left(\frac{J+1}{2J+1}\right)^{1/2}j_{J+1}(qr_i)[Y_{J+1}(\hat{\mathbf{r}}_i)\otimes\nabla_\xi]_{JM} +\left(\frac{J}{2J+1}\right)^{1/2}j_{J-1}(qr_i)[Y_{J-1}(\hat{\mathbf{r}}_i)\otimes\nabla_\xi]_{JM}-(q/8)j_J(qr_i)Y_{JM}(\hat{\mathbf{r}}_i)\right\}, \tag{14}$$

where the second and third terms in Eq. (11) are the Darwin-Foldy and spin-orbit terms, $\kappa_i=(2.79,-1.91)$ for (p,n), and M_N is the nucleon mass. The last terms in Eqs. (12) and (13) are second-order contributions to the transverse current. The RCCSM is a nonrelativistic model, and it seems consistent to stop at terms of order $1/M_N^2$. With $(q/M_N)^3=0.15$ for $q=500$ MeV/c, a rough limit of approximately 400 or 500 MeV/c would be placed on the possible momentum transferred; however, comparisons are included below to data beyond that range. The nucleon form factors F_1 and F_2 are taken from the three-pole approximation of Ref. [16] and are a function of q_μ^2. These equations include two target recoil corrections. The first is the term multiplying $q/8$ in Eq. (14); the second involves the gradient in Eqs. (12) and (13), $\nabla_\xi=(3/4)\nabla_{r_i}$, for ^{4}He.

To see where the recoil terms enter the multipoles, one can look at the direct matrix element of $\exp(-\mathbf{q}\cdot\mathbf{y}_4)\mathbf{p}_4'$, where the 4 indicates that particle number 4 is struck. The momenta are measured in the laboratory frame, and the coordinate could be measured from any fixed laboratory position, but will be taken from the initial position of the target for convenience. The matrix element between initial and final states becomes

$$\int \psi_1'^*(\xi_1)\psi_2'^*(\xi_2)\psi_3'^*(\xi_3)e^{-i\mathbf{R}\cdot\mathbf{p}_B'}e^{-i\mathbf{q}\cdot\mathbf{y}_4} \times\mathbf{p}_4'\psi_1(\xi_1)\psi_2(\xi_2)\psi_3(\xi_3)e^{i\mathbf{R}\cdot\mathbf{p}_B}\prod_j d\mathbf{y}_j . \tag{15}$$

One wishes to express the wave functions in terms of their momentum distributions,

$$\psi_1\psi_2\psi_3e^{i\mathbf{R}\cdot\mathbf{p}_B}=(2\pi)^{-6}\int \Phi(\mathbf{p}_1,\mathbf{p}_2,\mathbf{p}_3,\mathbf{p}_4) \times\exp\left(i\sum_j \mathbf{y}_j\cdot\mathbf{p}_j\right)\prod_j d\mathbf{p}_j , \tag{16}$$

so that $\psi_1'^*\psi_2'^*\psi_3'^*\mathbf{p}_4'$ may be written in terms of a coordinate space operation. However, the convenient momentum variables are those conjugate to $\boldsymbol{\xi}_1$, $\boldsymbol{\xi}_2$, $\boldsymbol{\xi}_3$, $\mathbf{R}$, which will be called $\mathbf{k}_1$, $\mathbf{k}_2$, $\mathbf{k}_3$, and $\mathbf{k}_4$. A transformation exists between the $\mathbf{p}_i$ and $\mathbf{k}_i$, and one has

$$\begin{aligned}\psi_1\psi_2\psi_3e^{i\mathbf{R}\cdot\mathbf{p}_B}&=(2\pi)^{-9/2}\int \phi_1(\mathbf{k}_1)\phi_2(\mathbf{k}_2)\phi_3(\mathbf{k}_3) \times\delta^3(\mathbf{k}_4-\mathbf{p}_B)\exp\left(i\sum_j \boldsymbol{\xi}_j\cdot\mathbf{k}_j\right)\prod_j d\mathbf{k}_j \\ &=(2\pi)^{-9/2}\int \phi_1(\mathbf{k}_1)\phi_2(\mathbf{k}_2)\phi_3(\mathbf{k}_3) \times\delta(\mathbf{k}_4-\mathbf{p}_B)\exp\left(i\sum_j \mathbf{y}_j\cdot\mathbf{p}_j\right)\prod_j d\mathbf{p}_j ,\end{aligned} \tag{17}$$

and therefore

$$(2\pi)^{-3/2}\Phi(\mathbf{p}_1,\mathbf{p}_2,\mathbf{p}_3,\mathbf{p}_4)=\phi_1(\mathbf{k}_1)d_2(\mathbf{k}_2)\phi_3(\mathbf{k}_3) \times\delta^3(\mathbf{k}_4-\mathbf{p}_B). \tag{18}$$

With $\mathbf{p}_4'=\frac{1}{4}\mathbf{k}_4'+\mathbf{k}_3'$ one has

$$\begin{aligned}&\psi_1'^*\psi_2'^*\psi_3'^*e^{-i\mathbf{R}\cdot\mathbf{p}_B'}\mathbf{p}_4' \\ &\quad=\{[\tfrac{1}{4}(-i\nabla_{\mathbf{R}})+(-i\nabla_{\xi_3})]\psi_1'\psi_2'\psi_3'e^{i\mathbf{R}\cdot\mathbf{p}_B'}\}^\dagger \\ &\quad=\{\tfrac{3}{4}(-i\nabla_{r_4})\psi_1'\psi_2'\psi_3'e^{i\mathbf{R}\cdot\mathbf{p}_B'}\}^\dagger \\ &\qquad+\tfrac{1}{4}\mathbf{p}_B'\psi_1'^*\psi_2'^*\psi_3'^*e^{-i\mathbf{R}\cdot\mathbf{p}_B'}.\end{aligned} \tag{19}$$

The ∇_{r_4} term may be moved to the initial state by integration by parts, and using $\mathbf{p}_B'=-\mathbf{q}$ one sees that the second term is entirely longitudinal, contributing to J_z, and is proportional to the Coulomb multipole.

The meson exchange currents included in this work are only the pionic and pair contributions developed in Ref. [17]. The matrix elements were evaluated in momentum space, since this procedure is much faster for the high oscillator principal quantum numbers contributing to the continuum, and the use of correlated wave functions in calculating the matrix elements in coordinate space produced relatively small changes [5]. Delta excitation diagrams were omitted because of their model dependence and their expected importance only in the dip region.

III. RESULTS

The RCCSM was employed previously in a variety of calculations involving nucleon knockout. The first of these calculations was for ^{4}He$(\gamma,p)^3$H [8]. It is worth returning to that calculation, because it provides one with a comparison to data at near zero momentum transfer. Figure 2 displays two theoretical curves and the data of Refs. [18–23]. The dashed line is calculated with the transverse nuclear current operators. The solid line is calculated in the long-wavelength approximation and with application of the continuity equation to convert the transverse nuclear current operators to Coulomb operators. The long-wavelength approximation is good to a few percent at the peak of the cross section, but the two calculations disagree. In fact, they disagree by more than the expected factor of $(E_\gamma^{\rm expt}/E_\gamma^{\rm th})^2=1.3$. The two calculations agree when pure harmonic oscillator wave functions are employed for the ground and excited states and $E_\gamma^{\rm expt}$ is set equal to $E_\gamma^{\rm th}=\hbar\omega$. The difficulty is that the RCCSM solution is an approximate solution to the Hamiltonian, dictated by the limited basis, and is not guaranteed to satisfy the continuity equation as discussed in Ref. [24].

One therefore sees that the transverse current is inadequate at very low momentum and energy transfer. The inclusive 180° (e,e') experiments of Ref. [25] allow one to pursue this problem as the momentum transfer increases. RCCSM calculations [6] have previously been compared to these data. In that investigation it was shown that orthogonality between initial and final states and that inclusion of the contribution of the recoiling residual nucleus was crucial to a description of the scattering process. However, the recoil correction factor of $\frac{3}{4}$ in Eq. (19) was not included. In that

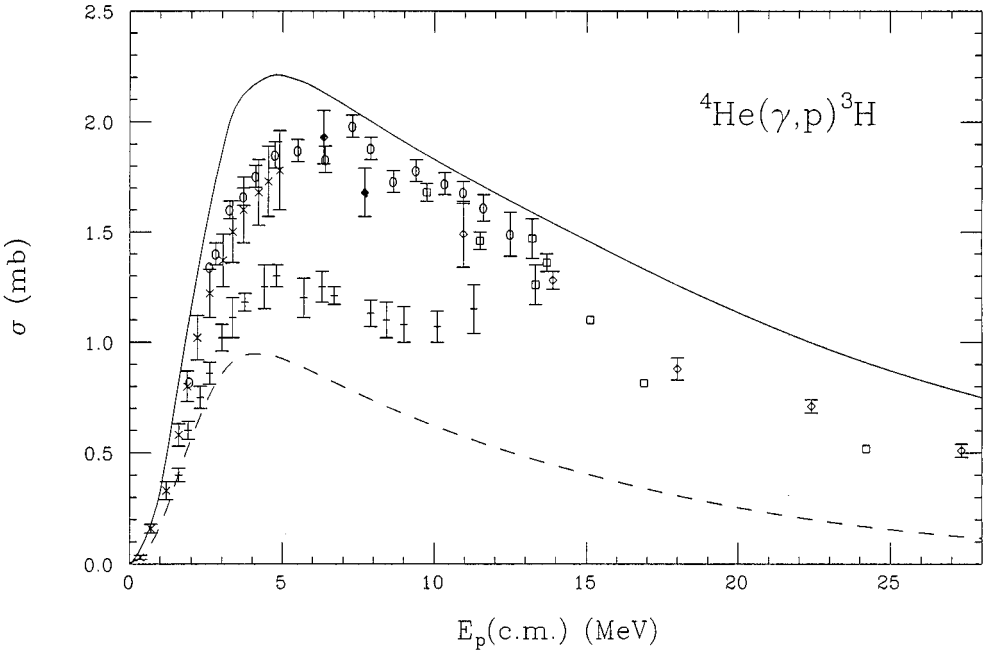

FIG. 2. Photodisintegration cross sections. Solid line is calculated with the transverse nuclear current operators; dashed line with Coulomb operators. Open circles, crosses, squares, diamonds, ×'s, and solid diamonds are data of Refs. [18], [19], [20], [21], [22], and [23], respectively.

work the multipole operators were derived with the standard assumption that the four-nucleon center of mass did not change. In addition, the nucleon form factors employed in this work are superior to the Gaussian form used in [6]. The resulting cross sections are reduced ~17%. They are shown in Fig. 3 where it can be seen that the cross sections, due entirely to the transverse response, are slightly low when compared with the data, but not by the factor of 2 seen in the (γ,p) calculation. The agreement is poorest at $q\approx360$ MeV/c, with the calculation being approximately 40% too small. These results are consistent with the (γ,p) findings if one assumes that the weakness is in the convective current. This is because the 2^- channel dominates at low q and is excited only by the magnetization current. The convective current was, of course, the main contribution to the (γ,p) cross section.

The inclusive results at higher q can be compared with the work of Refs. [26] and [27]. In both of these works the longitudinal and transverse responses were separated according to

$$\frac{d^2d}{d\Omega\ dE}=\sigma_{\text{Mott}}[v_L R_L(q,\omega)+v_T R_T(q,\omega)], \qquad (20)$$

which neglects the recoil factor $1/[1+(k'-k\cos\theta)/E'_B]$.

The complete calculation is shown in Fig. 4 as the solid line and is compared to the data of Ref. [26]. The calculation is also shown in Fig. 5, where it is compared to the data of Ref. [27]. The missing strength in the calculated transverse response at $q=300$ MeV/c and low energy transfer are evident in Fig. 4 and show approximately the same depletion as when compared against the 200 MeV data in Fig. 3. This is less evident in the data of Ref. [27] shown in Fig. 5, and it would be helpful to know which data set is correct. The depletion in the low energy region continues at $q=400$ and 500 MeV/c.

One could blame the lack of theoretical strength near the

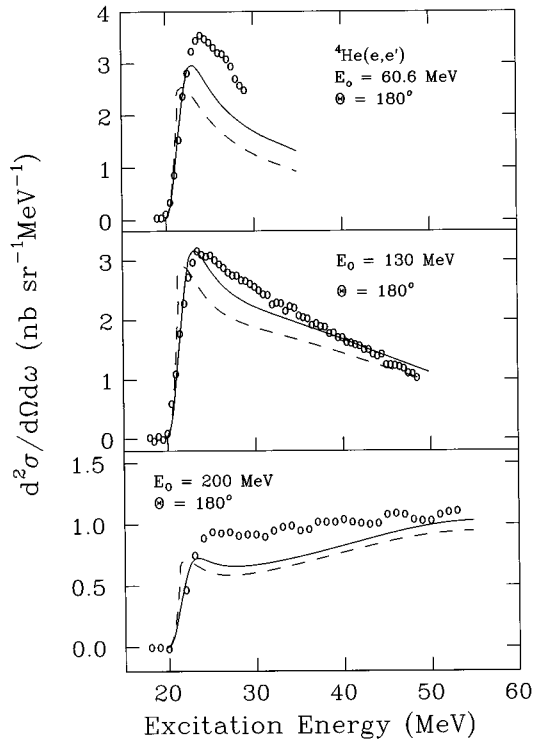

FIG. 3. Solid lines are full calculation; dashed lines omit transitions from channels which do not correspond to the entrance channel. Data are from Ref. [25].

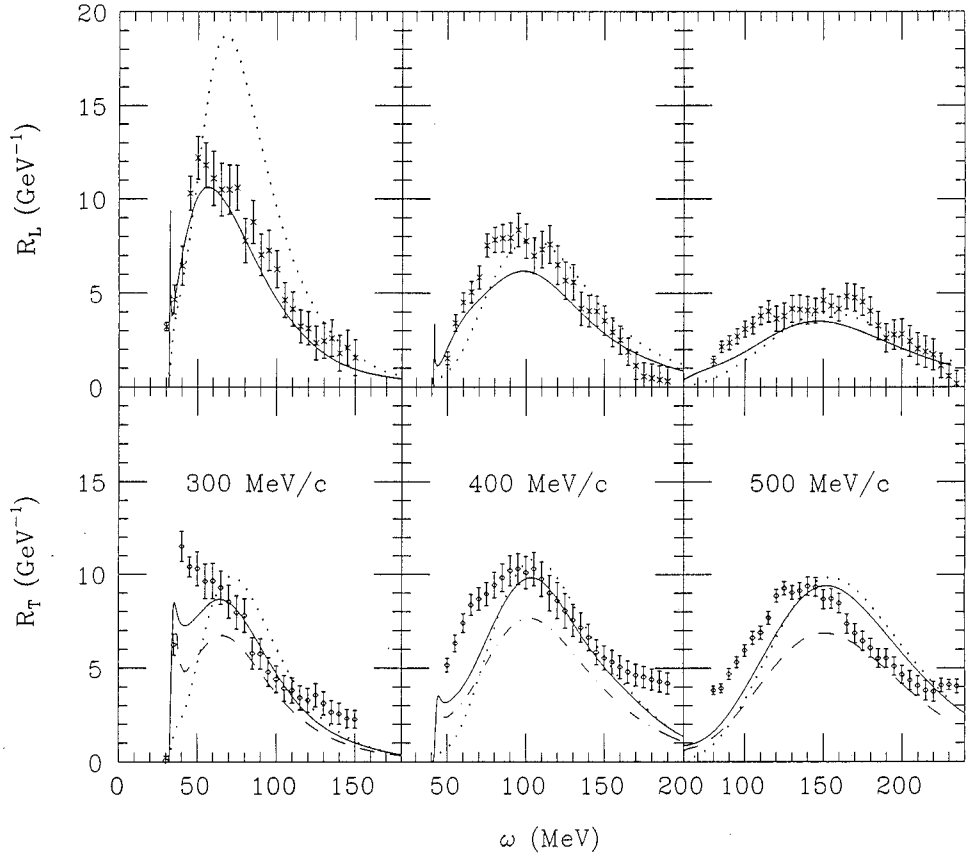

FIG. 4. Solid lines are full calculations; dotted lines are near-plane-wave calculations; dashed lines omit meson exchange currents from full calculations. Data are from Ref. [26].

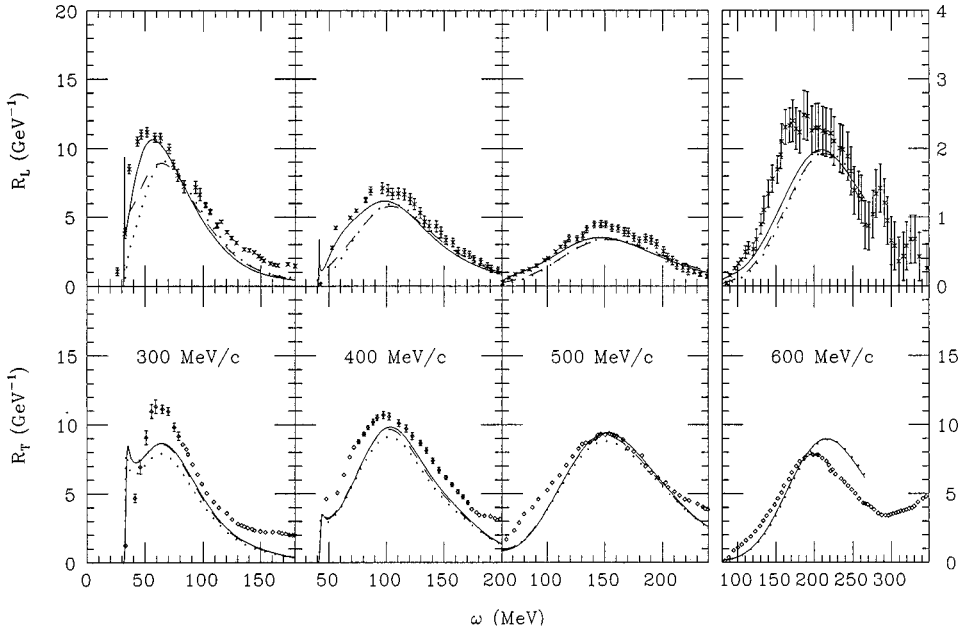

FIG. 5. Solid lines are full calculations, and dashed lines omit transitions from spin-flip channels. In all panels except R_T q=600 MeV/c, dotted lines omits transitions from flip and charge exchange channels. In R_T q=600 MeV/c panel, dotted line omits second-order contribution to nuclear current. Data are from Ref. [27].

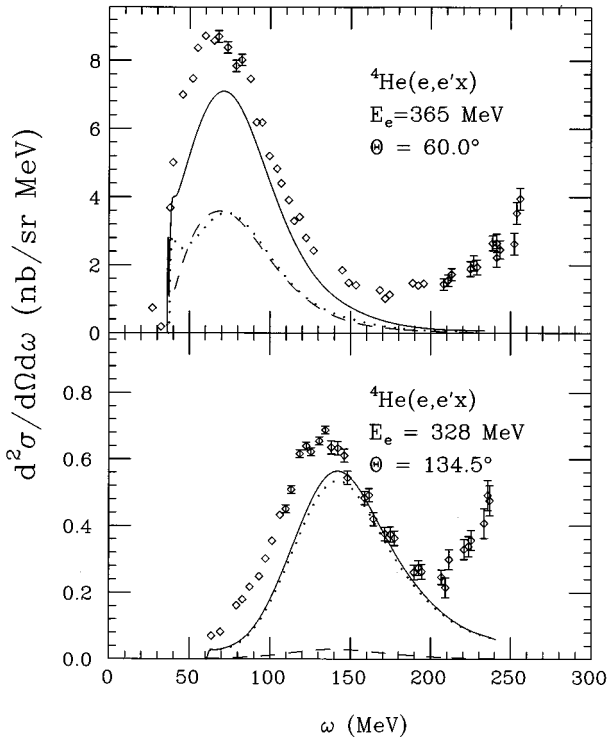

FIG. 6. Solid lines are full calculations, dashed lines are the longitudinal contributions, and dotted lines are transverse contributions. Data are from Ref. [26].

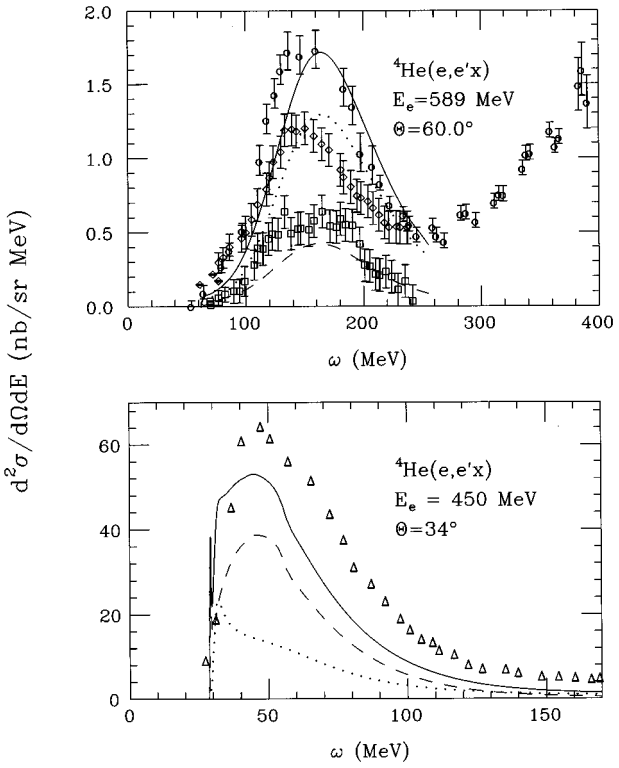

FIG. 7. Solid lines are full calculations, dashed lines are longitudinal contributions, and dotted lines are transverse contributions. Circle, diamonds, and squares are total, transverse, and longitudinal data from Ref. [26] and triangles are total from Ref. [27].

quasielastic peak on the fact that the experiment includes all inclusive channels, and the calculation includes only the two-body proton and neutron channels [28]. However, at low energy transfer, one expects the proton and neutron channels to dominate. Therefore in this region, E_x=20 to 45 MeV, the calculated transverse strength is low. This is most likely due to not having an exact solution to the Hamiltonian, a hypothesis which could be tested by adding more complicated configurations to the model.

Comparisons have also been made to the excitation functions used in extracting the experimental response functions. Examination of Figs. 6 and 7 demonstrates that the calculated cross sections which are dominated by the transverse response show a weakness in the low energy regions. In fact, it appears the strength has been pushed to higher energies, again an indication of missing configurations.

Whereas one sees consistency between data sets in identifying the behavior of the calculated versus experimental transverse response, the longitudinal response is more difficult to characterize at low momentum transfer. The ^{4}He$(\gamma,p)^3$H calculation with Coulomb matrix elements is very nearly what one would have expected from the model. The 1^- states do seem to come somewhat lower in energy in the calculation than in the data. This is in contrast to the ^{3}H$(p,n)^3$He analyzing power–polarization data [8] which suggest that the theoretical 1^- states are at the correct positions. More significantly, the calculated cross section is only about 10% too high. This could easily be argued away as the lack of D-state configurations in the ground state, whose inclusion would reduce the photoexcitation strength. One would conclude, based on ^{4}He$(\gamma,p)^3$H, that the Coulomb matrix elements at low q are reasonable. However, comparison with low q electroexcitation cross sections in the regions dominated by the longitudinal response is inconclusive. An examination of the q=300 MeV/c response in Figs. 4 and 5 suggests that agreement with data is good, but agreement with individual cross sections is sporadic.

If one first looks at the cross section in Fig. 8 from Ref. [29], it would appear that the longitudinal response is well described at $q\approx$230 MeV/c. The nature of the 0^+ peak was analyzed within the RCCSM in Ref. [5] and the q dependence of the calculation followed that of the data. The predominantly 1^- background also seems to look like the data, except perhaps that it rises too quickly, much like the (γ,p) cross section. However, if one looks at the exclusive measurements of Ref. [30] at $q\approx$77 MeV/c, the agreement is very poor. The integrated cross sections and angular distributions are shown in Figs. 9 and 10. Although the shapes are correct, the theoretical curves require a multiplicative factor of 0.52. This is somewhat surprising, because the RGM calculation reported in Ref. [30] agrees perfectly with the data. Since the RCCSM and RGM are similar calculations, one would have expected similar results. This is one indication that the present RCCSM calculation is showing a size effect. The calculated rms radius of ^{4}He is 1.71 fm, while the experimental value is 1.67 fm.

However, if one compares to the E_e=169 MeV measurement [31], the agreement with the RCCSM is again reasonable at $q\approx$103 MeV/c, as shown in Fig. 11. Many cross sections were measured in Ref. [31]. Samples of comparisons with calculated cross sections are shown in Figs. 12 and

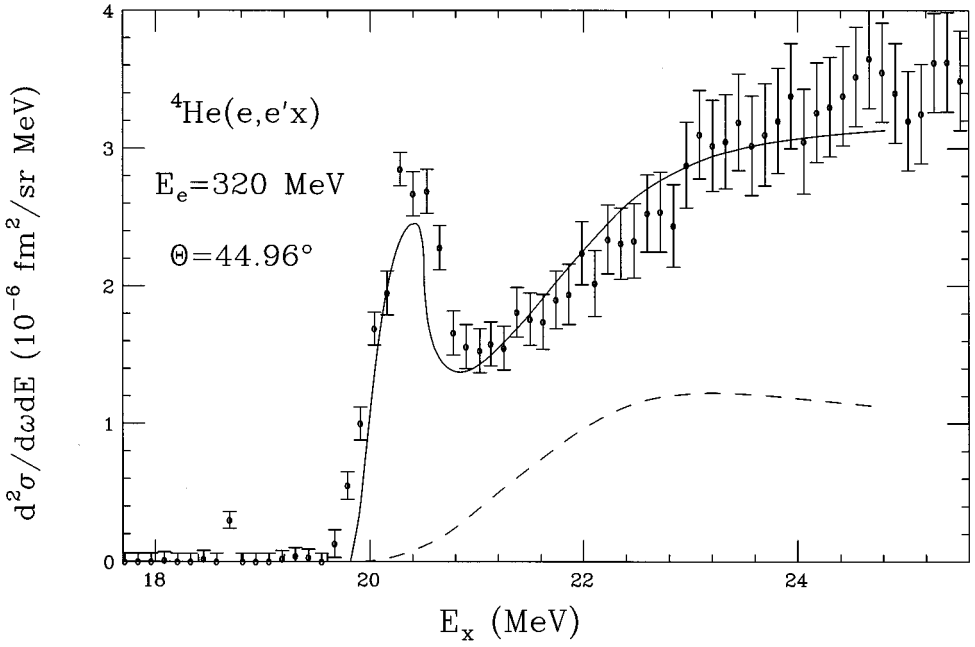

FIG. 8. Solid line is full calculation; dashed line is transverse only. Data are from Ref. [29].

13. A summary comparison is given in Fig. 14 where the calculated longitudinal response function for the dominant 1^- contribution is shown as a function of q and at a fixed excitation energy of E_x=24.8 MeV. Also plotted are experimental points determined by $R_L(1^-)\sigma_{\rm expt}/\sigma_{\rm th}$. The datum from Ref. [29] is represented as a square, that from Ref. [30] as a circle, and those of Ref. [31] as ×'s. Although it is difficult to see a consistent trend in the data, the calculated 1^- longitudinal response function appears to be too large at very low q. This would be inconsistent with the (γ,p) results, unless the (γ,p) data of Ref. [19] were correct.

At higher q the longitudinal response can be characterized by comparing again to the response functions of Refs. [26] and [27] in Figs. 4 and 5. The calculated longitudinal responses are approximately 10–20 % lower at the quasielastic peak. This is not a desirable outcome if, as suggested in Ref.

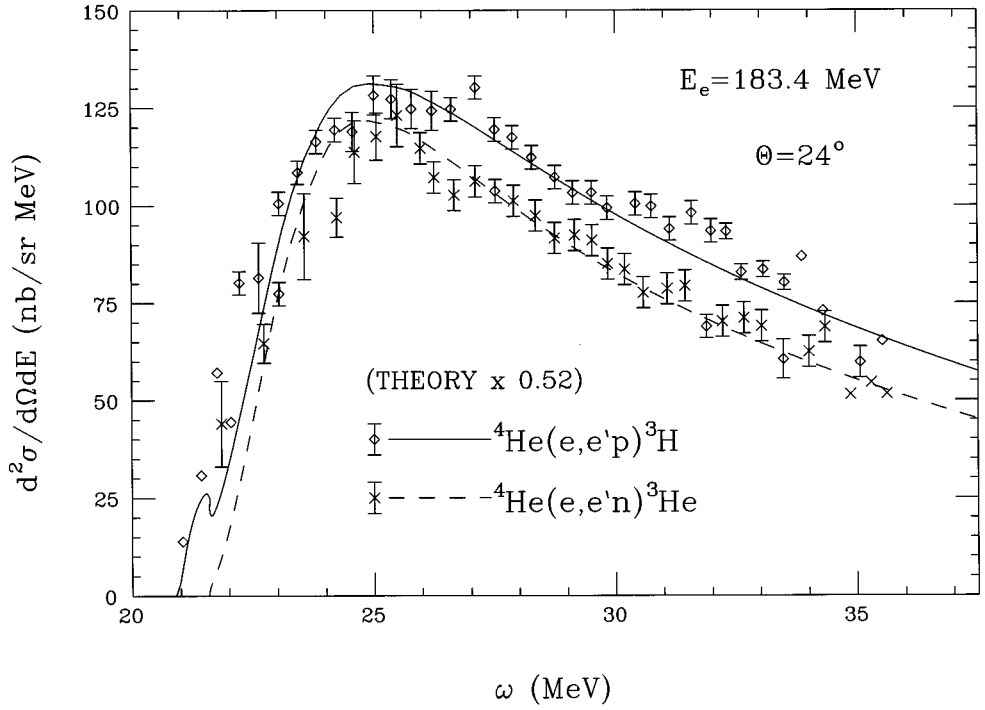

FIG. 9. Integrated cross sections. Solid line and diamonds are for ^{4}He($e,e'p$)^{3}H; dashed line and crosses are for ^{4}He($e,e'n$)^{3}He. Data are from Ref. [30]. Full calculations have been multiplied by 0.52.

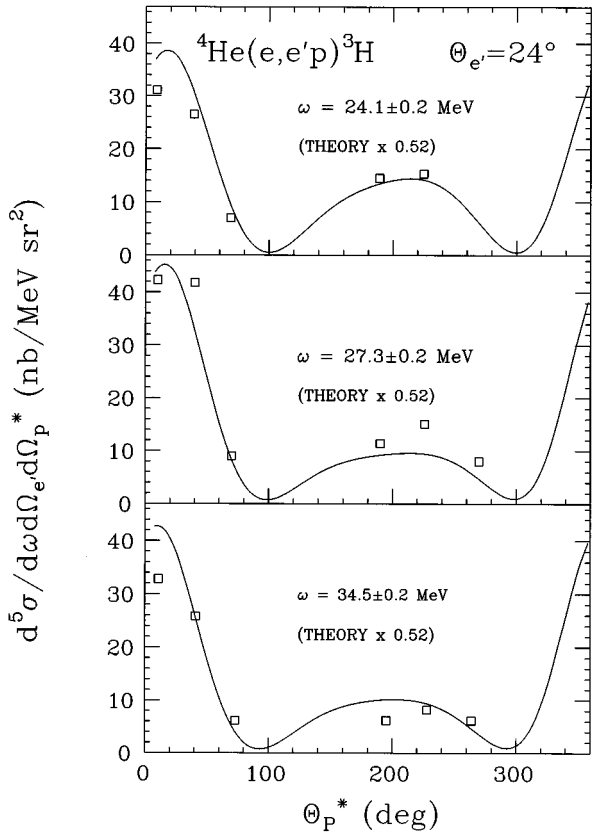

FIG. 10. Angular distributions of protons. Solid lines are full calculations multiplied by 0.52. Data are from Ref. [30].

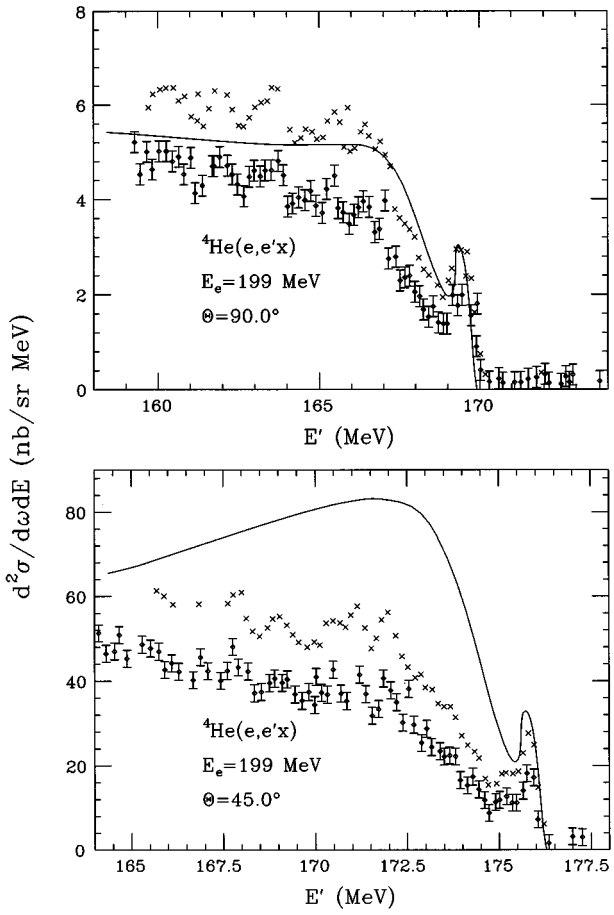

FIG. 12. Inclusive cross sections at E_e=199 MeV. Solid lines are full calculations. Crosses are uncorrected data; diamonds have radiative corrections. Data are from Ref. [31].

[28], only about half of the inclusive cross sections are due to the *p* and *n* channels. Overall, the longitudinal responses tend to have a more consistent relationship to the experimental values than the transverse responses.

A number of calculations are shown in Figs. 4 and 5. The solid lines are the complete calculations in both figures. In Fig. 4 the dotted line represents a near-plane-wave calculation in that it was calculated with the full Coulomb potential but only 10% of the nuclear potential. The procedure for determining the *S* matrix in this work [32] has some difficulty determining a perfectly vanishing phase shift, so the potential was not set exactly to zero. The dotted line looks very much like the plane-wave calculations in other works

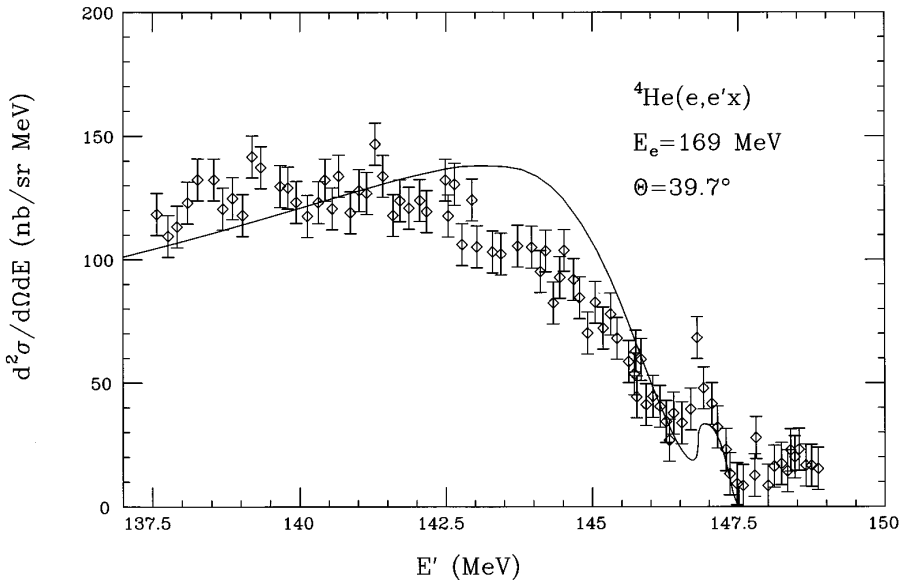

FIG. 11. Inclusive cross section at E_e=169 MeV. Solid line is full calculation. Data are from Ref. [31].

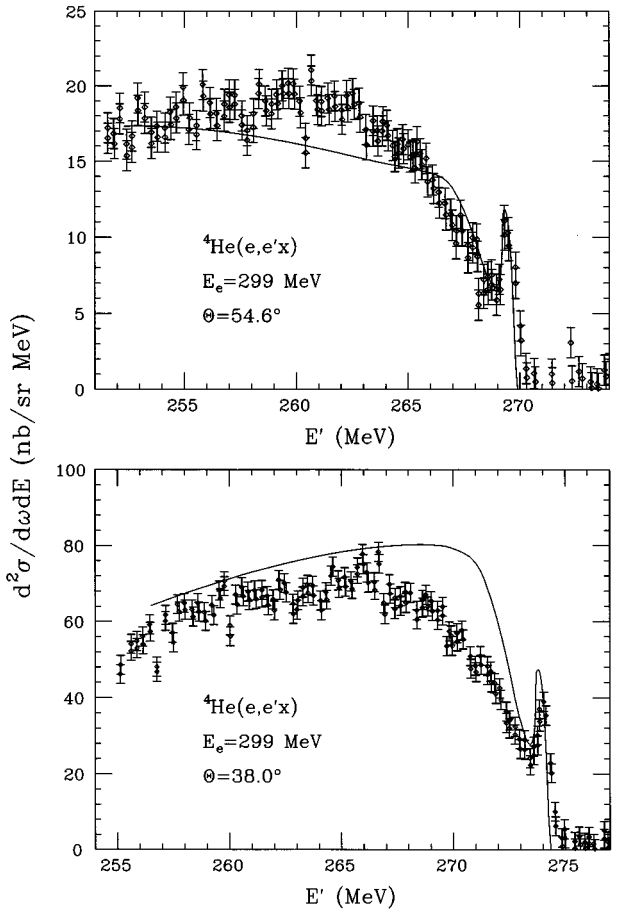

FIG. 13. Inclusive cross sections at E_e=299 MeV. Solid lines are full calculations. Data are from Ref. [31].

[26,33]. Agreement with the full calculation is reasonable at higher q, but at low q and ω the final state interactions reduce the calculate response by a factor of 2 and shift the strength to lower energies. The effects of final state distortions are small at high q and ω because the high partial waves provide large contributions, and they have small phase shifts. The exclusion of meson exchange currents is shown as the dashed line in Fig. 4 and they provide approximately 20% of the transverse response.

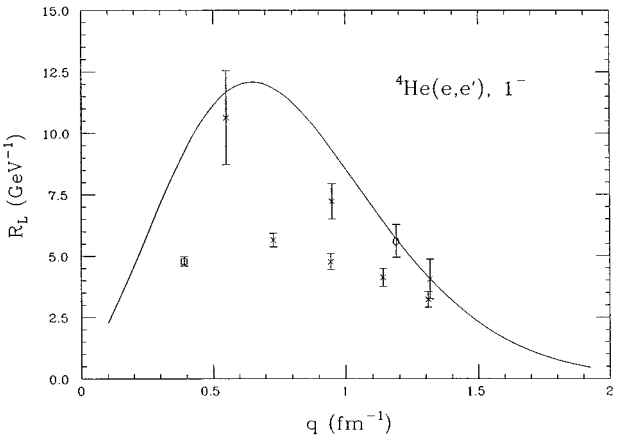

FIG. 14. Longitudinal response for 1^- channel at E_x=24.8 MeV as a function of q. Square, circle, and crosses are derived from data of Refs. [29], [30], and [31], respectively.

In Ref. [34] it was shown that coupling to the neutron channels could have a significant effect on the $(e,e'p)$ cross section. Therefore in that reference the neutron channels were included by describing the final states with the Lane model. This is an indication of the inadequacy of performing calculations with optical model wave functions for the final states. The RCCSM allows one to test the effects of omitted channels by setting the appropriate transition matrix elements to zero. As an example, the dashed lines in Fig. 5 are equivalent to a Lane model calculation in that all transition matrix elements which did not have the same j-j coupled quantum numbers as the outgoing channel were set to zero. The effect is significant, even at q=400 MeV/c, and indicates the importance of spin-channel coupling. Also, the effect is confined primarily to the longitudinal response.

The dotted lines in all but the R_T, q=600 MeV/c panel of Fig. 5 are the equivalent of distorted-wave calculations with optical model wave functions. This is accomplished by setting to zero all transition matrix elements from the charge exchange channels in addition to those which do not have the j-j coupled quantum numbers of the outgoing channel. Therefore the outgoing channel has the correct phase shift, but the channels which couple to it cannot contribute to the transition. This is the situation when all channel coupling is represented by an absorption. One sees that omission of charge exchange channels affects both the longitudinal and transverse responses at low q and ω.

An obvious problem develops in the q=600 MeV/c response functions. Most notable is the difference between the experimental and calculated quasielastic peak positions. This range of ω and q is certainly at the limit of applicability for the RCCSM with its nonrelativistic kinematics and simple ground state structure. In addition, the Δ excitation and heavy meson exchange currents will have contributions in this region. It would be difficult to extract one reason for the discrepancy, since it is most likely a combination of omissions which contribute. For instance, the dotted line in the R_T, q=600 MeV/c panel of Fig. 5 corresponds to a calculation which omits the second-order contribution to the transverse current. Inclusion of these terms pushes the calculation back toward the data, but certainly not far enough.

The second-order contributions to the nuclear current operators raise an ambiguity in these calculations, in that one must make some decision about the off-shell prescription. For the responses in Figs. 4 and 5 one must insert k_0-k_0' for ω appearing in Eqs. (12) and (13). But for the exclusive reactions, one can substitute $(M_N^2+p^2)^{1/2}-(M_N^2+p_m^2)^{1/2}$, where $\mathbf{p}_m$ is the missing momentum, $-\mathbf{q}-\mathbf{p}$. This procedure is used in all exclusive calculations below.

The exclusive experiments allow one to test the hypothesis that some of the missing strength in the calculations in Figs. 4 and 5 is due to channels other than $(e,e'p)$ and $(e,e'n)$. Cross sections for $(e,e'p)$ as a function of the missing momentum also provide information on the proton momentum distribution in the target. The data of Refs. [34] and [35] fall in the momentum and energy transfer range considered in this paper. Shown as $\times$'s in Fig. 15 are the experimental cross sections from Ref. [34]. They were taken under two kinematical conditions to cover a wide missing

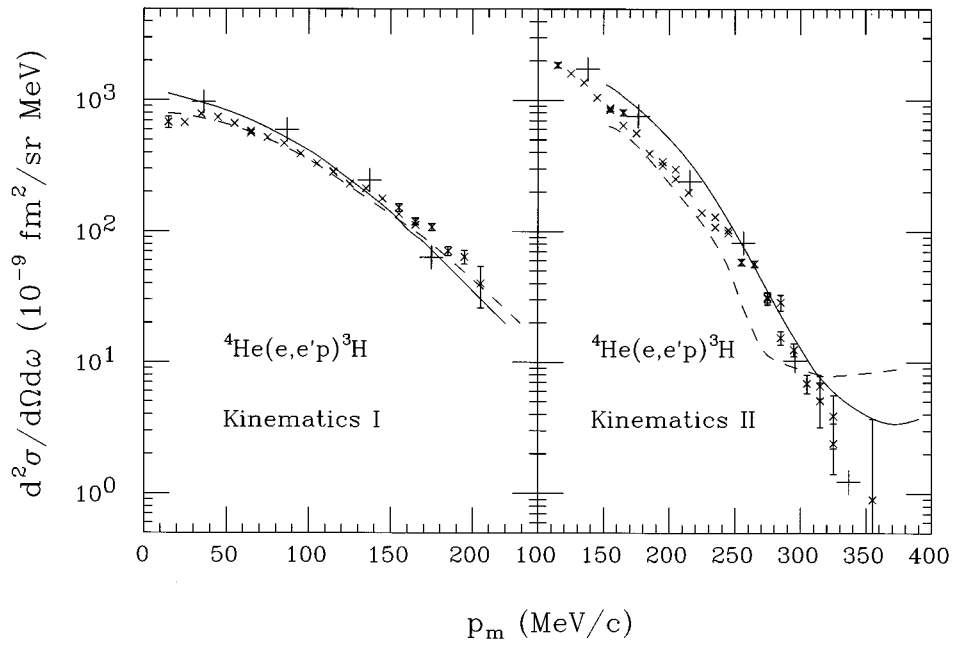

FIG. 15. Exclusive cross sections as a function of missing momentum. Data from Ref. [34] are shown as ×'s; calculated points are shown as crosses. Calculations of Schiavilla and Laget are shown as solid and dashed lines, respectively [34].

momentum range. For kinematics I q was approximately 431 MeV/c and for kinematics II it was approximately 250 MeV/c. The relative proton-^{3}H center of mass kinetic energy $T_{\text{c.m.}}$ was approximately 75 MeV in both. In this range one would expect the RCCSM to do well since it is still producing reasonable nucleon scattering cross sections. The crosses in Fig. 15 are the calculated cross sections at the kinematic points provided in Ref. [34]. The calculation agrees reasonably well with the data and does not show the unusual behavior at high missing momentum evident in the calculations reported in Ref. [34]. Two of these calculations are reproduced as dashed and solid lines in Fig. 15.

Data for other kinematic conditions were also reported in Ref. [34]. Plotted in Fig. 16 are these cross sections divided by the calculated cross sections. The points are plotted as letters corresponding to the notation in Ref. [34]. The points are plotted as a function of both q and $T_{\text{c.m.}}$. Agreement is generally good, except that for these data, it appears that agreement becomes worse as $T_{\text{c.m.}}$ increases. Also plotted in Fig. 16 are the points corresponding to the cross sections of

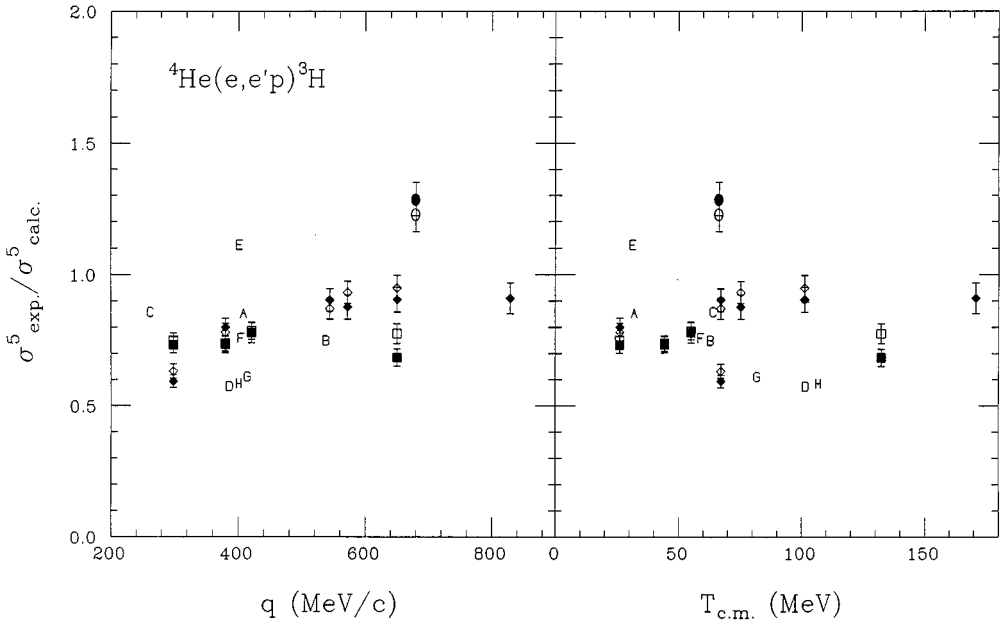

FIG. 16. Experimental divided by theoretical cross sections. Letters A–H represent data of Ref. [34]; solid squares, diamonds, and circles represent forward scattering data of Ref. [35] at p_m=30, 90, and 190 MeV/c; open squares, diamonds, and circles represent backward scattering data.

Ref. [35]. In Ref. [35] cross sections corresponding to the same values of q and ω were measured for both forward and backward electron scattering angles. Points plotted as solid squares, diamonds, and circles are for forward scattering at p_m=30, 90, and 190 MeV/c, respectively. Points plotted as open squares, diamonds, and circles are for backward scattering at p_m=30, 90, and 190 MeV/c, respectively. Corresponding pairs lie within error bars of each other, which is a tribute to the experiment. Less hopeful are points A and E of Ref. [34] which have similar q and ω, but one is overpredicted by the calculation and one is underpredicted. Whereas point A lies close to the points with similar energy and momentum transfer derived from the data of Ref. [35], point E is far outside the group and is likely spurious.

When all points are considered, the trend in $T_{\text{c.m.}}$ is not evident. As a function of q, the points indicate a tendency for the calculation to overpredict more at low q than at high q. This would be consistent with the comparisons made at low q for the inclusive calculations.

Combining these inclusive results with the exclusive results above, one can make an estimate of the contribution of single-nucleon knockout to the quasielastic peak. At q=400 MeV/c the calculations account for ~90% of the inclusive quasielastic peak. The exclusive calculations at $q\approx$400 MeV/c and $\omega\approx$100 MeV overpredict by ~25%. This would indicate that one-third of the quasielastic peak corresponds to processes other than one-nucleon knockout. This value of one-third stays fairly constant over the range q=300 to 500 MeV/c. This is not inconsistent with the 40–50 % estimates in Ref. [28], given that a larger nucleus, ^{12}C, was investigated in that analysis.

In Ref. [35] extractions were made for effective longitudinal and transverse spectral functions S_L and S_T. The calculated cross sections from this present work were treated in the same manner as the experimental cross sections in extracting theoretical values for S_L and S_T. Comparisons are made in Fig. 17, where the experimental values at p_m=30 MeV/c are plotted as squares, the p_m=90 MeV/c points are plotted as diamonds, and the p_m=190 MeV/c points are plotted as crosses. The theoretical points are plotted as circles and those corresponding to the same p_m are connected by solid straight lines. The trend again seems to be, at least at high missing momentum, that low q calculations overpredict the data less than high q calculations. The conjecture that this behavior is largely due to the large rms radius (1.71 fm) of the RCCSM ground state is supported by the calculations reported in Ref. [35], where the Argonne v14 calculation, with its rms radius of 1.71 fm, produced larger spectral functions at p_m=30 MeV/c than the Urbana v14 calculation, with its rms radius of 1.62 fm.

Also shown as circles in Fig. 17 are the ratios of experimental values for S_L/S_T to calculated values. Since the points do not show a preference for being above or below unity, one must conclude that no evidence for suppression of the longitudinal spectral function appears in this present work. Of course, one does notice the one point in which the calculation appears to be off by a factor of 2. The present calculations provide no reason for this data point to be in error, but it is suggested that the error bars are considerably larger than quoted.

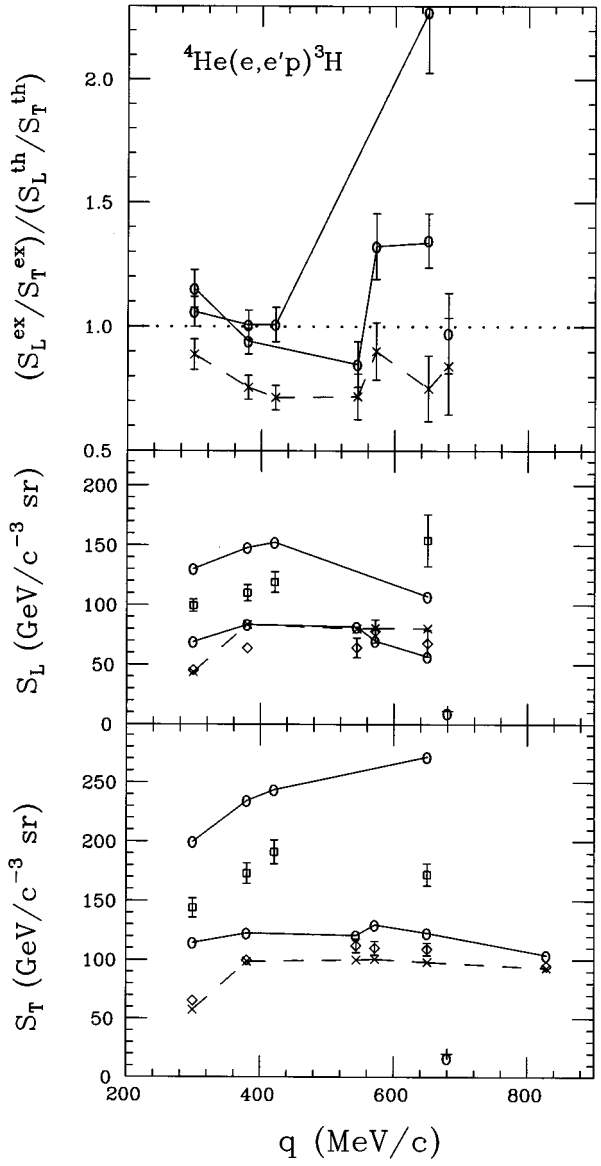

FIG. 17. Spectral functions for ^{4}He($e,e'p$)^{3}H. Squares, diamonds, and crosses represent p_m=30, 90, and 190 MeV/c data of Ref. [35]. Circles are for present calculation. Points at the same missing momenta are joined by straight lines. ×'s are calculated in Ref. [37].

A summary of the exclusive results as compared to the data in Ref. [35] is shown in Table I. Results are given for the full, meson exchange currents omitted, no second-order correction to the transverse current operator, spin-flip channel transitions omitted, spin-flip and charge exchange channel transitions omitted, near-plane-wave, and no continuity equation calculations. This last column corresponds to calculating $\langle J_z\rangle$ directly from Eq. (9) and not relating it to $\langle\rho\rangle$ via the continuity equation. It provides some measure of the effect of violating the continuity equation. Even though $\langle J_z\rangle$ differs greatly from $\langle(q_0/q)\rho\rangle$, and therefore the continuity equation does not hold, $\langle J_z\rangle$ is small compared to $\langle\rho\rangle$, and the effect is small.

The low q and low ω transverse strength observed in the exclusive measurements appears to be opposite to that ob-

TABLE I. Cross sections for ^{4}He$(e,e'p)^3$H in nb sr^{-2} MeV^{-1}.

Experiment	Full	No exch. currents	No 2nd trans.	No spin coupling	No chan. coupling	Plane wave	No cont. equation
1*f* 46.5±0.9±1.5	62.0	59.3	62.1	59.5	60.6	73.5	65.1
1*b* 2.65±0.05±0.09	3.61	3.26	3.61	3.52	3.46	3.99	3.69
2*f* 36.1±0.7±1.2	48.9	47.0	48.9	48.1	48.7	54.3	51.8
2*b* 2.65±0.05±0.09	3.61	3.27	3.59	3.56	3.52	3.79	3.68
3*f* 23.8±0.5±0.8	30.3	28.6	30.3	29.7	29.9	32.2	32.2
3*b* 2.92±0.06±0.10	3.75	3.39	3.72	3.70	3.67	3.87	3.84
4*f* 3.53±0.07±0.12	4.55	3.66	4.47	4.46	4.42	4.48	4.76
4*b* 1.35±0.03±0.04	1.97	1.55	1.93	1.95	1.93	1.95	2.01
5*f* 24.6±0.5±0.9	38.9	35.2	39.6	35.6	35.8	39.4	41.1
5*b* 1.29±0.03±0.04	2.18	2.05	2.25	2.18	2.15	2.90	2.27
6*f* 19.4±0.4±0.7	24.9	22.0	24.8	22.8	23.1	23.0	26.1
6*b* 1.29±0.03±0.04	1.61	1.40	1.60	1.58	1.56	1.48	1.63
7*f* 4.28±0.09±0.15	4.91	4.28	4.84	4.74	4.74	4.77	5.18
7*b* 1.11±0.02±0.04	1.23	1.06	1.21	1.22	1.22	1.15	1.25
8*f* 3.61±0.07±0.12	3.88	3.29	3.80	3.76	3.75	3.58	4.08
8*b* 1.04±0.02±0.04	1.19	0.991	1.15	1.18	1.18	1.11	1.21
9*f* 2.02±0.04±0.07	2.13	1.72	2.07	2.08	2.06	1.98	2.23
9*b* 0.730±0.015±0.024	0.807	0.643	0.778	0.802	0.796	0.760	0.817
10*b* 0.423±0.008±0.015	0.465	0.296	0.369	0.457	0.447	0.441	0.471
11*f* 0.289±0.006±0.011	0.235	0.183	0.228	0.230	0.230	0.189	0.245
11*b* 0.115±0.002±0.004	0.0936	0.0741	0.0897	0.0960	0.0964	0.0784	0.0946

served in the inclusive measurements in that, from Fig. 17, the transverse response at $q=299$ MeV/c, $p_m=30$ MeV/c, and $\omega=57.8$ MeV is overpredicted in the calculation by about 30%; however, an average from Figs. 4 and 5 indicates that the experimental transverse response for $q=300$ MeV/c at $\omega=57.8$ MeV is still higher than the calculation by about 20%. It is difficult to imagine that two-nucleon knockout could account for such a large difference at such a low energy transfer, corresponding to $E_x=45.9$ MeV. However, as mentioned above, the shapes of the two inclusive analyses in Figs. 4 and 5 differ greatly in this region. The 180° data in Fig. 3 tend to support the shape of the analysis in Fig. 4; however, in Fig. 3 the calculation and experiment agree at $E_x=45.9$ MeV. One would certainly like to have the inclusive, experimental situation clarified, most likely by additional 180° data, which can be incorporated into the response analyses. If, indeed, the exclusive and inclusive measurements are vastly different, one would be very interested in pursuing the mechanism.

IV. COMPARISON TO OTHER CALCULATIONS

Several calculations have been reported for the electroexcitation of ^{4}He in the $q>300$ MeV region. Often quoted are calculations of Laget [34,36,37] and the Argonne-Urbana-CEBAF collaboration [35,38,39]. Such calculations employ sophisticated solutions from realistic NN interactions for the $A=3$ and 4 ground states. However, one must deal with the difficulty of calculating the ^{3}H-^{4}He overlap function and with the lack of equivalent solutions to the continuum problem. The continuum problem may be dealt with in a plane-wave approximation, distorted-wave approximation, or Lane model. Corrections to plane-wave calculations have also been calculated with a diagrammatic approach [34]. In Ref. [2] the spectral functions were calculated via a RPA, and in Ref. [3] they were calculated within the RGM.

Certainly, all of the calculations show that the plane-wave approximation is inadequate at all but the highest momentum and energy transfers. Meson exchange currents gave important contributions to all calculations. The calculations of Schiavilla [39] and Laget [37], shown as solid and dashed lines in Fig. 15, are examples where model dependent exchange currents are included. For Ref. [39] meson exchange currents increased the cross section by more than 50% for $p_m>200$ MeV/c. This compares well with the results of this present work. However, the exchange currents of Ref. [37] turned destructive near $p_m=300$ MeV/c. It would appear that one is seeing the result of the model dependence of Δ excitation and ρ exchange graphs. These graphs were omitted from the present calculation because of their model dependence, and because they would become important in the dip region where the RCCSM would not be expected to do well because of its nonrelativistic kinematics.

The calculations of Ref. [37] were also compared to the data of Ref. [35]. These are shown as crosses and connected with dashed lines in Fig. 17. These results agree much better with the data than do the RCCSM results. However, only the $p_m=90$ MeV/c results were quoted in Ref. [37], and other calculations [35] with the Argonne v14 potential have produced cross sections which are larger than the data at $p_m=30$ MeV/c. In addition, the calculations in Ref. [37] have difficulty describing the data of Ref. [34] for kinematics II as mentioned above and shown in Fig. 15.

Plotted as ×'s in Fig. 17 are results of Ref. [37] for the ratio of experimental to theoretical ratios S_L/S_T. Here the

present calculation agreed reasonably well with the experimental values except for the one point discussed above. However, the points from Ref. [37], calculated with $J_z=(q_0/q)\rho$, are all less than unity, which would indicate a suppression of the longitudinal response. Too many of the circles from the present calculations are consistent with unity to make this conclusion. In other works the RGM calculation [3] indicates a suppression, and the distortion-corrected calculations in Ref. [35] lean that way, while the RPA [2] calculation indicates a larger experimental as compared to theoretical longitudinal spectral function. One can only conclude that if the longitudinal spectral function is suppressed, it is not by much, and the situation is not clear.

From the present work one has seen that the p-n channel coupling is important at low momentum and energy transfer. In Ref. [39] the effect was 3% for kinematics I and 13% for kinematics II for the calculations in Fig. 15. Given the kinematic range, this is not inconsistent with the present calculation. The coupled channels calculations in Ref. [37] indicate a p-n channel effect which is large and nearly independent of energy transfer, while the diagrammatic calculations show a decrease in importance with increasing energy transfer, as does the present calculation.

Most of the calculations listed above do a reasonable job of agreeing with the data in Ref. [34] when plotted against the missing momentum. Interestingly, the RGM calculation [4] and the RCCSM calculations do as well as or better than those calculations employing a more sophisticated ground state. The RGM calculation employs a very simple form for the $A=3$ and 4 ground states, in fact, nearly the same as the RCCSM. The RCCSM uses a more realistic NN interaction, and the RGM calculation allows a sum of two Gaussians for the $A=3$ system instead of one, but the virtues of translational invariance, antisymmetrization, channel coupling, exact extraction of the ^{3}H-^{4}He overlap, and a consistent Hamiltonian for both the ground and continuum states hold for both models. Therefore it appears that comparisons to exclusive experiments are presently limited in their ability to distinguish among theoretical ground states by a lack of a continuum solutions with equivalent sophistication.

V. CONCLUSIONS

Calculations were performed for the electroexcitation of ^{4}He in the framework of the RCCSM. The versatility of the model allows one to investigate reactions at a variety of values for the energy and momentum transfer. Agreement with data is generally as good as or better than for calculations employing more sophisticated ground state wave functions. Two regions where the RCCSM departs from data are the inclusive transverse response at low energy transfer and the exclusive longitudinal response at very low momentum transfer. Whereas the disagreement in the longitudinal response is likely due to a size effect, the disagreement in the transverse response is unexplained. Inclusion of 180° scattering experiments in the extraction of low q response functions would provide helpful information in quantifying the problem, and addition of more complicated configurations in the RCCSM may provide a possible solution.

This work was supported by the U.S. National Science Foundation under Grant No. PHY-202938.

[1] T. deForest, Jr. and J. D. Walecka, Adv. Phys. **15**, 1 (1965).
[2] F. A. Brieva and A. Dellafiore, Phys. Rev. C **36**, 899 (1987).
[3] M. Buballa, S. Drozdz, S. Krewald, and A. Szczurek, Phys. Rev. C **44**, 810 (1991).
[4] T. Warnamm and K. Langanke, Phys. Lett. B **273**, 193 (1991).
[5] D. Halderson, M. Yu, and J. Yu, Phys. Rev. C **39**, 336 (1989).
[6] D. Halderson, Phys. Rev. C **45**, 42 (1992).
[7] A. Picklesimer, J. W. Van Orden, and S. J. Wallace, Phys. Rev. C **32**, 1312 (1985).
[8] D. Halderson and R. J. Philpott, Nucl. Phys. **A321**, 295 (1979); **A359**, 365 (1981).
[9] D. Halderson, J. Phys. G **20**, 1461 (1994).
[10] G. Bertsch, J. Borysowicz, H. McManus, and W. G. Love, Nucl. Phys. **A284**, 399 (1977).
[11] D. Halderson, R. J. Philpott, J. A. Carr, and F. Petrovich, Phys. Rev. C **24**, 1095 (1981).
[12] T. W. Donnelly and J. D. Walecka, Annu. Rev. Nucl. Sci. **25**, 329 (1975).
[13] D. M. Brink and G. R. Satchler, *Angular Momentum* (Oxford University Press, Oxford, 1968).
[14] K. W. McVoy and L. Van Hove, Phys. Rev. **125**, 1034 (1962).
[15] S. Boffi, C. Giusti, and F. D. Pacati, Nucl. Phys. **A336**, 416 (1980).
[16] T. Janssens, R. Hofstadter, E. B. Hughes, and M. R. Yearian, Phys. Rev. **142**, 922, (1966).
[17] D. J. Dubach, J. H. Koch, and T. W. Donnelly, Nucl. Phys. **A279**, 279 (1974).
[18] W. G. Meyerhoff, M. Suffert, and W. Feldman, Nucl. Phys. **A148**, 211 (1970).
[19] G. Feldman, M. J. Balbes, L. H. Kramer, J. Z. Williams, and H. R. Weller, Phys. Rev. C **42**, R1167 (1990).
[20] A. N. Horbunov, Phys. Lett. **27B**, 436 (1968); JETP Lett. **8**, 188 (1968).
[21] W. R. Dodge and J. J. Murphy II, Phys. Rev. Lett. **28**, 839 (1972).
[22] J. E. Perry and S. J. Bame, Phys. Rev. **99**, 1368 (1955).
[23] J. R. Calarco, S. S. Hanna, C. C. Chang, E. M. Diener, E. Kuhlman, and G. A. Fisher, Phys. Rev. C **28**, 483 (1983).
[24] J. M. Eisenberg and W. Greiner, *Microscopic Theory of the Nucleus* (North-Holland, Amsterdam, 1976).
[25] A. Hotta *et al.*, Phys. Rev. C **38**, 1547 (1988).
[26] K. F. von Reden *et al.*, Phys. Rev. C **41**, 1084 (1990).
[27] A. Zghiche *et al.*, Nucl. Phys. **A572**, 513 (1994).
[28] L. B. Weinstein and G. A. Warren, Phys. Rev. C **50**, 350 (1994).
[29] G. Köbschall *et al.*, Nucl. Phys. **A405**, 648 (1983).
[30] M. Spahn *et al.*, Phys. Rev. Lett. **63**, 1574 (1989).
[31] R. Frosch *et al.*, Nucl. Phys. **A110**, 657 (1968).
[32] R. J. Philpott, Nucl. Phys. **A243**, 260 (1975).

[33] C. Ciofi degli Atti, Nucl. Phys. **A463**, 127c (1987)
[34] J. F. J. van den Brand *et al.*, Nucl. Phys. **A534**, 637 (1991).
[35] J. E. Ducret *et al.*, Nucl. Phys. **A556**, 373 (1993).
[36] J. M. Laget, Nucl. Phys. **A497**, 391c (1989).
[37] J. M. Laget, Nucl. Phys. **A579**, 333 (1994).
[38] R. Schiavilla, V. R. Pandharipande, and R. B. Wiringa, Nucl. Phys. **A449**, 219, (1986).
[39] R. Schiavilla, Phys. Rev. Lett. **65**, 835 (1990).